Identification of Abnormal Cervical Regions from Colposcopy Image Sequences

Mingpei Liang[1], Gaopin Zheng[2], Xinyu Huang[1], Gaolin Milledge[1], Alade Tokuta[1]
[1]North Carolina Central University
1801 Fayetteville Street
Durham, NC 27707, USA
{mliang, huangx, gzheng, atokuta}@nccu.edu
[2]Shenzhen Luohu Maternity and Infant Healthy Institute
2013 Taibai Rd, Luohu
Shenzhen, Guangdong 518999, P.R. China
gaopinzheng@yahoo.com.cn

ABSTRACT

Cervical cancer is the third most common cancer in women worldwide and the leading cause of cancer death in women of the developing countries. Cancer death rate can be greatly reduced by regular screening. One of the steps during a screening program is the detection of the abnormal cells that could evolve into cancer. In this paper, we propose an algorithm that automatically identifies the abnormal cervical regions from colposcopy image sequence. Firstly, based on the segmentation of three different image regions, a set of low-level features is extracted to model the temporal changes in the cervix before and after applying acetic acid. Second, a support vector machine (SVM) classifier is trained and used to make predictions on new input feature vectors. As the low-level features are very insensitive to accurate image registration, only a rough normalization step is needed to sample image patches. Our preliminary results show that our algorithm is accurate and effective. Furthermore, our algorithm only needs to sample patches from six image frames within a five-minute time period. Hence, the proposed algorithm also could be applied to improve the accuracy of the mobile telemedicine for cervical cancer screening in low-resource settings.

Keywords

Colposcopy Image Processing, Support Vector Machine, Feature Extraction, Cervical Cancer

1. INTRODUCTION

Cervical cancer is the commonest cause of cancer death among women in developing countries [QBP+12]. Cervical cancer is preceded by pre-malignant cervical intraepithelial neoplasia (CIN). In order to prevent cervical cancer, the accurate diagnosis of cancer cells and abnormal regions followed by appropriate therapy is necessary. Colposcopy is a widely used diagnostic method to detect CIN and cervical cancer. Once the abnormal region is identified, the samples of cells are often taken from the cervix for an abnormal cytological screen (i.e., Papanicolaou smear). During the colposcopic exam, application of 3-5% acetic acid to the cervix can turn abnormal and metaplastic epithelia to white, while normal cervical squamous epithelia remain pink. It is believed that the amount of whiteness is positively associated with the severity of cervical intra-epithelial neoplasia (CIN) [GKL+11, QGR+11]. Therefore, the whiteness is considered as one of major characteristics to detect cancer and pre-cancerous regions. Other features, such as morphologic characteristics around precursor lesions [Lan05] and vascular patterns, can also be used for identification. However, they may not be salient sometimes and thus may not be as effective as whiteness of cervical epithelia.

In order to minimize subjective variability among physicians and improve reliability and repeatability of diagnosis, a sound computer aided image processing algorithm that could combine all possible features is highly desirable. Such a system can enhance the power of existing colposcopes and would make them immediately useful in low-resource areas of the developing countries [SCN+09].

In this paper, we propose an image processing and statistical learning procedure to identify abnormal

regions in colposcopy images. Firstly, we notice that the cervical surface has limited and very similar texture patterns. Some regions could also be very smooth. Thus, many image registration techniques that rely on detection of feature points could fail since feature points often cannot be detected and tracked over image frames consistently. Our algorithm is particularly useful for the situation when the accurate image registration cannot be achieved. Second, a set of low-level features is extracted to model color and thickness changes in the cervix. The Support Vector Machine [CV95] is applied for the classification. Based on our preliminary experiments, accurate classification rate can be achieved by sampling only six images within a five-minute time interval. We believe that the proposed algorithm could be adopted to improve the diagnostic performance of the mobile telemedicine for cervical cancer screening [QGR+11]. As number of current training data is limited and more data is often needed to improve robustness of classification performance, we also plan to label and train on a large set of image sequences in the future.

The remainder of this paper is organized as follows. Section 2 describes related work. Our proposed algorithm is given in section 3. Experiments in section 4 show the success classification rates. The conclusion is given in section 5.

2. RELATED WORKS

The research in this area is limited and current methodologies [AK07, AKL11, SCN+09] follow the standard pipeline of medical image processing.

The first step is the image registration. In [AK07], feature points are detected using the Harris corner detector. This detector can detect changes in the first derivative of an image. Other similar feature points detector, such as SIFT [Low04] and MSER [FL07], also could be applied with similar detection performance. Matched feature points in two consecutive image frames are used to estimate a 2D transformation between them. However, many colposcopy images contain limited and very similar texture patterns, thus, matching of feature points often are not robust and accurate.

The registration algorithm based on a rigid transformation including translation and in-plane rotation is described in [AKL11]. Since a larger image region is used for registration, the performance could be better than the algorithms based on detection of feature points. However, during the colposcopic exam, other rigid transformations of the camera are also very common, such as scaling and out-of-plane rotation. Moreover, the cervix itself could have nonlinear deformations. Hence, only translation and in-plane rotation are unable to model the transformations in all the image frames. If all the transformations are considered, the process could be time-consuming and often done offline. The speed of the registration algorithm in [AKL11] is approximately 10 minutes for two image frames.

In the feature extraction step, whiteness is measured based on changes of saturation values in [AKL11]. Other features, such as morphologic features and vascular patterns, are not modeled and measured in most existing algorithms.

3. OUR ALGORITHM

According to [GZH04], the cervix area could be divided into three regions, squamous epithelium that remains pink after acetic acid application, columnar epithelium that is a dark and irregular region between endometrium and squamous epithelium, and the acetowhite region that is the region turned into white after acetic acid application. Figure 1 shows the structure of cervix area. The region of specular reflection is also large and keeps changing its position due to movements of colposcopy and cervix.

Our algorithm can be divided into five modules: 1) Specular reflection removal; 2) Segmentation of different image regions; 3) Normalization; 4) Extraction of low level features; 5) Classification using Support Vector Machine. The normalization step is mainly used to sample image patches for the SVM prediction. For the training purpose, this step could be skipped. Figure 2 gives an overview of the

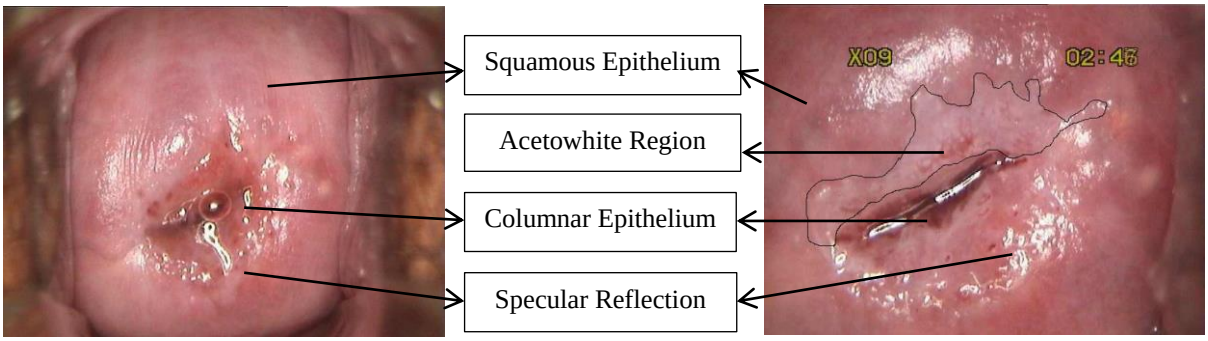

Figure 1: Image before acetic acid application (Left). Image enlarged 9 times and taken 2 minutes 46 seconds after acetic acid application (Right).

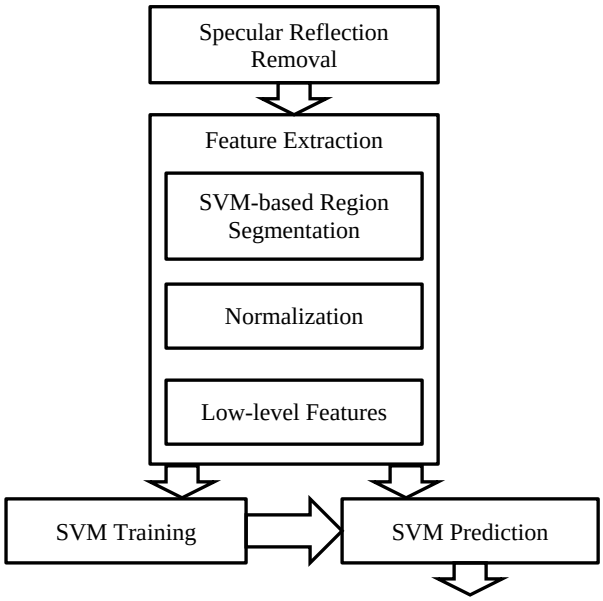

Figure 2: Outline of the algorithm.

algorithm.

3.1 Specular Reflection Removal

Specular reflections are random patterns that would greatly affect the estimation of low level features. Therefore, it is important to remove them before any further processing. Specular reflections are the brightest pixels in the image and the region containing specular reflections usually is smooth. We use a bi-linear interpolation method to fill the reflections. First, we compute a binary reflection map by a threshold (i.e., 250 in our algorithm). For each reflection pixel (x_0, y_0), we then search four envelop points that are outside the region of reflections, I_l, I_r, I_t, I_b, along vertical and horizontal directions. The reflection pixel is filled by

$$I_{(x_0,y_0)} = \frac{I_l \cdot (x_r - x_0) + I_r \cdot (x_0 - x_l) + I_b \cdot (y_0 - y_t) + I_t \cdot (y_b - y_0)}{2(x_r - x_l) + 2(y_b - y_t)}$$

where $(x_r, y_0), (x_l, y_0), (x_0, y_b), (x_0, y_t)$ are the pixel coordinates of four envelop points.

3.2 Feature Extraction

Given an image patch, since the accurate registration is not easy to obtain, we employ the use of low-level features that are not sensitive to the accuracy of registration. As mentioned in section 1, there are mainly three characteristics used to determine whether the patch contain abnormal cells and cancer cells: whiteness changes of metaplastic epithelia, morphologic changes around precursor lesions, and changes of vascular regions. To model these characteristics, we propose six low-level features based on color, edge information, and texture information.

3.2.1 SVM-based Region Segmentation

In order to measure the color changes correctly, we need to separate the regions with bleeding tissues that often become worse after acetic acid application. Otherwise, these bleeding regions could skew the actual whiteness changes. We sampled dozens of pixels in bleeding regions, the dark region of columnar epithelium, and other regions. Figure 3 shows the color distributions of three regions.

Firstly, we build a classifier to separate bleeding regions and the dark region of columnar epithelium. Given training set of colors $x_i \in R^3$ $(i = 1, \dots, N)$ and corresponding labels $y_i \in \{-1,1\}$ (i.e., bleeding region and other two regions), the SVM training algorithm is used to find the best decision plane that separates the largest subset of the training colors correctly and maximizes the margin between sampled colors. A new color sample x is classified by the decision plane, given by

$$y(x) = \sum_{i=1}^{N} \alpha_i y_i k(x, x_i) + b$$

where α_i denotes the Lagrange multipliers, b is a bias term, N is the number of training colors, and $k(x, x_i)$ is the kernel function. α_i and b are estimated from the SVM training stage and a linear kernel function is used.

Similarly, another SVM classifier is built to separate the dark region of columnar epithelium and the third region.

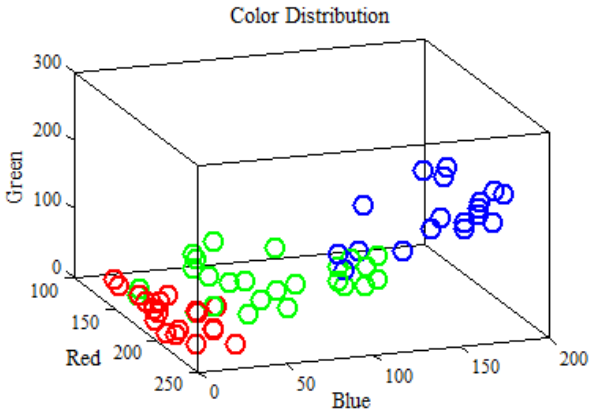

Figure 3: Color distributions of three different regions. (Red) samples from bleeding regions. (Green) samples from dark region of columnar epithelium. (Blue) samples from other regions.

3.2.2 Image Normalization for Prediction

In order to obtain six temporal image patches for the SVM predication, which contain roughly same cervical area, a normalization step is used. Unlike the image registration, this normalization step only gives a quite rough alignment among six image frames.

First, we use the SVM classifier learned in previous section to estimate the dark regions of columnar epithelium. The largest connected component in the central area of the image is considered as the dark region of columnar epithelium. The centroid of the connected component is used to compute the translation among image frames. The 1st principal component from principal component analysis (PCA) is used to compute the rotation and scaling parameters. Therefore, these image frames are roughly aligned together and we can easily extract feature vectors from corresponding image patches for predictions.

3.2.3 Low-level Features

After the separation between bleeding regions and other two regions, 1st quartile, median, and 3rd quartile of pixel colors are computed in both regions respectively. These two 3×1 vectors are used to represent colors of two regions in the image patch of each image frame.

The edges are a strong clue for the morphologic changes around precursor lesions. A Canny edge detector [Can86] is applied to the image patch and the edge length, which is the number of edge pixels in the image patch, is computed.

Texture feature could be used to measure thickness of boundaries of precursor lesions since these boundaries often become thick and obvious after acetic acid application. We compute the mean value of gradient magnitudes in the image patch, $\frac{1}{N}\sum_{x_i,y_i}\sqrt{J_{x_i}^2 + J_{y_i}^2}$, where N is the total number of pixels in the patch and (J_{x_i}, J_{y_i}) is the gradient for the ith pixel. If the cervix surface is smooth, then the mean magnitude is small in general.

Figure 4 shows the temporal distributions of median color in the non-bleeding region, edge length, and the texture feature. These distributions are the average distributions of 20 sampled patches for each image frame. From these distributions, we can find that median of green channels of abnormal regions tends to increase after acetic acid application. The distribution of median of blue channels is also very similar to Figure 4(a). The medians of red channels tend to remain same for both regions as shown in Figure 4(b). As a result, the color of the abnormal region tends to turn into white. We also notice that edge length and texture features also increase in the abnormal regions as shown in Figure 4(c) and 4(d), which indicates the morphologic changes. Since the distribution for a single patch could vary, it is necessary to concatenate all the features together to form a more robust feature vector. Thus, there is an 8×1 vector for each image patch and 6 image patches; and thus, the size of the feature vector is 48×1.

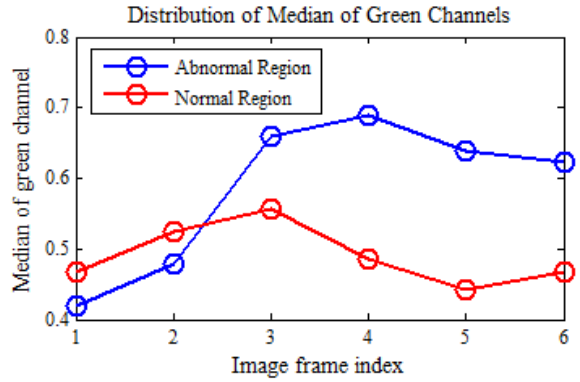

(a)

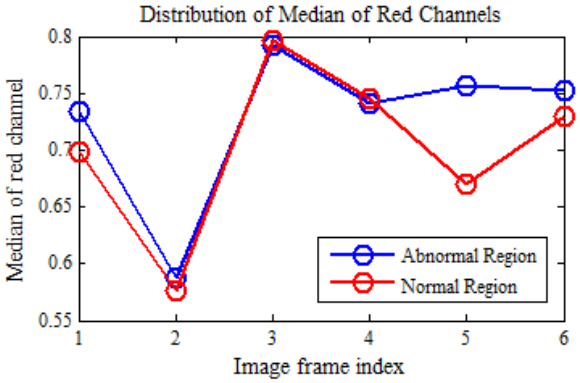

(b)

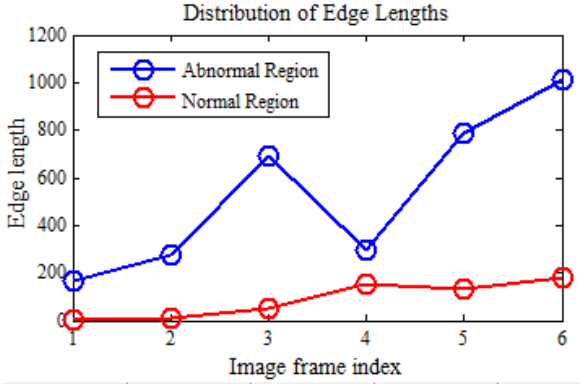

(c)

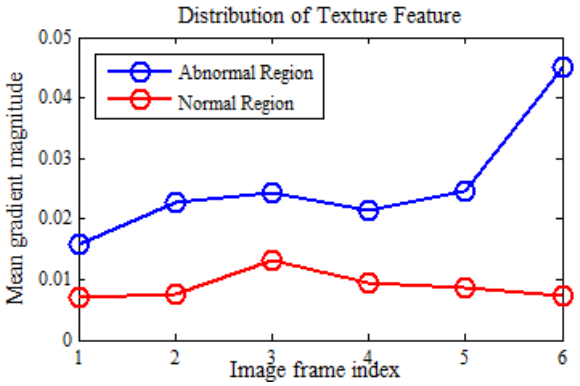

(d)

Figure 4: Temporal distributions of different features.

3.3 SVM Classification

In the training stage, we sample a set of image patches that contain abnormal regions and normal regions. The image patch size is consistent with the actual size for the Papanicolaou smear. Due to the irregular shape of the abnormal region and scaling factor of each image frame, the resolution of the image patches varies. We manually select and crop the corresponding image patches in the six image frames. Every set of six image patches contains the same cervix tissues. As the accurate image registration is not required, these patches often have different image appearances with unknown in-plane and out-of-plane rotations, translation, and scaling. However, this would not affect the classification performance since our low-level features are not sensitive to these linear or nonlinear transformations.

Given $N \times M$ training data $x_i \in R^M$ $(i = 1, \dots, N, M = 48)$ and observations $y_i \in \{-1,1\}$ (i.e., abnormal region and normal region), the SVM algorithm estimates the hyperplane to separate two different results. Three different kernel functions, linear kernel, radial basis function (RBF) kernel, and polynomial kernel, are evaluated.

4. EXPERIEMNTS

4.1 Datasets

We manually cropped 48 sets of positive rectangular patches from cervical lesion region from 12 patients with various degrees of cervical dysplasia. We also cropped approximately 40 sets of negative patches from normal cervical regions from these patients. Each set of positive or negative patches contains patches cropped from six temporal image frames. These data sets are used for the SVM training stage. The patch resolution ranges from 67×67 to 118×168, which is caused by different zooming factor of the colposcopy and different distances between cervix and the colposcopy. The patch size is also selected so that the cells in this region can be sampled for the subsequent Papanicolaou smear. Figure 5 and Figure 6 show two sets of image patches. We can find that the patch resolutions are not exactly same. However, they cover roughly the same cervical region. As the low-level features are not sensitive to the accurate image registration, our classification performance is not affected.

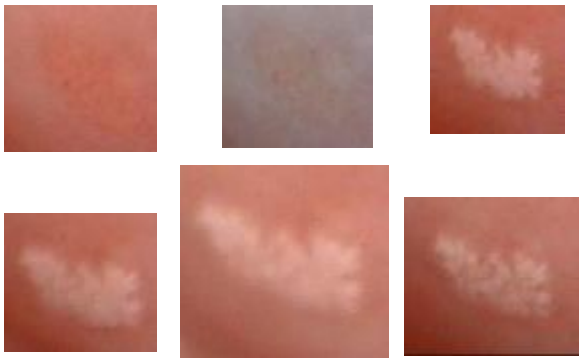

Figure 5: Example of one set of image patches with abnormal cells. They are arranged from left to right and from top to bottom in ascending order of time.

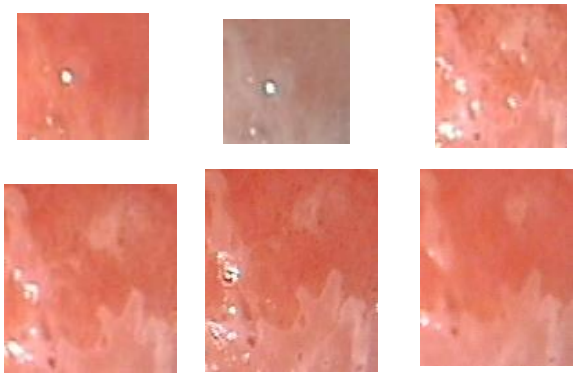

Figure 6: Example of one set of image patches with normal cells. They are arranged from left to right and from top to bottom in ascending order of time.

To evaluate prediction performance, we further sampled 30 sets of positive patches and 27 sets of negative patches.

4.2 Classification Performance

Table 1, 2, and 3 show the success classification rates when color features, edge features, and texture features are used separately. The performances are quite similar for three different kernels. Table 4 shows the success classification rate when all the features are combined. The highest rate from the testing dataset is 94.6% when the linear kernel is used. These experiments demonstrate the effectiveness of our proposed algorithm. Moreover, the simple linear kernel gives the best performance.

Table 1: Classification performances when only the features that model color changes are used.

Kernel	Success Classification Rate
Linear	83.9%
RBF	85.7%
Polynomial	85.7%

Table 2: Classification performances when only the edge features are used.

Kernel	Success Classification Rate
Linear	81.9%
RBF	85.1%
Polynomial	71.4%

Table 3: Classification performances when only the texture features are used.

Kernel	Success Classification Rate
Linear	87.2%
RBF	89.3%
Polynomial	83.4%

Table 4: Classification performances all the features are used.

Kernel	Success Classification Rate
Linear	94.6%
RBF	85.7%
Polynomial	89.3%

5. CONCLUSION AND FUTURE WORK

In this paper, we proposed a classification algorithm that can detect the abnormal cells in the cervical region. Our algorithm requires no accurate image registration. The low-level features are extracted and used as input in the SVM classification. The experiments show that the success classification rate could reach 94.6%. In the future, we would like to continue labeling data and further evaluate our algorithm using a large scale database. Since our algorithm is efficient and can run in real time, it would be promising to implement a real-time interactive diagnose system.

6. ACKNOWLEDGMENTS

The authors acknowledge support of the National Science Foundation HRD 0833184. The training and testing data sets are labeled by the physicians from Shenzhen Luohu Maternity and Infant Healthy Institute in Shenzhen, P. R. China.

7. REFERENCES

[AK07] Juan D. Garcá Arteaga and Jan Kybic "Automatic landmark detection for cervical image registration validation", *Proc. SPIE* 6514, *Medical Imaging 2007: Computer-Aided Diagnosis,* 65142S (March 31, 2007)

[AKL11] J. D. Garcia A-Arteaga, J. Kybic, and W. Li, "Automatic colposcopy video tissue classification using higher order entropy-based image registration," *Comput. Biol. Med.*, vol. 41, pp. 960-970, 2011.

[Can86] J. Canny, "A computational approach to edge detection", *IEEE Transaction on Pattern Analysis and Machine Intelligence*, Vol: 8, Issue 6, pp 679-698, 1986

[CV95] Corinna Cortes and Vladimir Vapnik, "Support-vecot networks", Machine Learning, Vol 20, Issue 3, pp 273-297, Spetember 1995

[FL07] P.E. Forssen and D.G. Lowe, "Shape descriptors for maximally stable extremal regions", *IEEE International Conference on Computer Vision*, pp 1-8, 2007

[GZH04] S. Gordon, G. Zimmerman, and H. Greenspan, "Image segmentation of uterine cervix images for indexing in PACS", *Computer-Based Medical Systems, 2004, CBMS 2004. Proceedings, 17th IEEE Symposium on*, June 2004

[Lan05] H. Lange, "Automatic glare removal in reflectance imagery of the uterine cervix," in *Proc. SPIE 5747, Medical Imaging*, 2005, pp. 2183-2192.

[Low04] David G. Lowe, "Distinctive image features from scale-invariant keypoints", International Jounral of Computer Vision, Vol 60, Issue 2, pp 91-110, November 22004

[QGR+11] Kelly E Quinley, Rachel H Gormley, Sarah J Ratcliffe, Ting Shih, Zsofia Szep, Ann Steiner, Doreen Ramogola-Masire, and Carrie L Kovarik, "Use of mobile telemedicine for cervical cancer screening", *Journal of Telemedicine and Telecare*, 2011

[QBP+12] M. K. Quinn, T. C. Bubi, M. C. Pierce, M. K. Kayembe, D. Ramogola-Masire, and R. Richards-Kortum, "High-Resolution Microendoscopy for the Detection of Cervical Neoplasia in Low-Resource Settings," *PLoS ONE*, vol. 7, p. e44924, 2012

[SCN+09] Y. Srinivasan, E. Corona, B. Nutter, S. Mitra, and S. Bhattacharya, "A Unified Model-Based Image Analysis Framework for Automated Detection of Precancerous Lesions in Digitized Uterine Cervix Images," *Selected Topics in Signal Processing, IEEE Journal of*, vol. 3, pp. 101-111, 2009.